

# New Antenna Designs to Boost the Plasma Density in Helicon Sources

Rayan AlSayed Ali<sup>1</sup>, Ghassan Antar<sup>1</sup>, and Joseph Costantine<sup>1</sup>, *Senior Member, IEEE*

**Abstract**—Plasma can be generated using radio frequency (RF) electromagnetic waves for a large variety of applications, such as energy and propulsion generation. Often, the desire is to achieve higher densities for given input power and helicon sources have demonstrated a high efficiency. The design of the antenna that couples the wave plays a major role in the efficiency of generating the plasma particles. Many geometries were studied and compared, but the relationship between the antenna characteristics and the plasma production is still missing. In this article, we identify the power-law dependence between the plasma density and the Gain of an antenna. The latter is determined using numerical simulations in a vacuum, whereas the former is acquired experimentally. The power-law dependence is obtained using four different antenna elements operating under the same experimental conditions on the Polaris linear plasma device. The design *a posteriori* of a new inductive antenna with a modified quadrifilar helix topology, exhibits not only a higher gain but also confirms the power law. The confirmation of this law will significantly impact the future of many technologies that leverage helicon plasmas.

**Index Terms**—Antenna design, antenna gain, helicon plasma, magnetized plasma devices, radio frequency (RF) antenna.

## I. INTRODUCTION

PLASMA generation in laboratories has a wide range of applications in a variety of fields like in nuclear fusion [1], space thrusters [2], and plasma processing [3]. A large number of studies are thus dedicated to the production of hot and dense plasma using electromagnetic waves. In 1997, a first review, done by Chen and Boswell [4] presented an account of the understanding of helicon waves and the experimental results. Later in 2015, Chen [5] gave another comprehensive summary of the physics of helicon discharges. In 2018, Shinohara [6] wrote an overview of the experimental results related to radio frequency (RF) sources and their applications.

The first helicon plasma source was achieved in an experiment conducted by Lehane and Thoneman [7]. Later on,

Boswell [8] and Scime *et al.* [9] obtained plasma densities as high as  $4 \times 10^{12} \text{ cm}^{-3}$  leading to the observation of the first “blue core” argon plasma. Chen [10] presented a theoretical explanation for the high efficiency of helicon waves by including both collisions and Landau damping and the results were elegantly exposed in his paper. However, it was shown that number of fast electrons was insufficient to provide all the ionization in a helicon discharge [11], [12]. Chen *et al.* [14] concluded that the Trivelpiece-Gould mode [13] could be the main ionization mechanism.

The literature is rich with experimental investigations of helicon plasma sources employing a variety of antennas that generate a perturbation in the form  $e^{(m\theta+kz-\omega t)}$ . The perturbation angular frequency is  $\omega$ ,  $z$  is the axial direction along which it has a wavenumber  $k$ . We have the mode number  $m$  in the azimuthal direction  $\theta$  that is set by the antenna shape. The values  $m = +1$  or  $-1$  correspond to a global right or left-hand rotation of the wave pattern for a static magnetic field.

Lehane and Thoneman [7] used a set of two-loop antennas to excite an  $m = 0$  and  $m = +1$  modes. The Boswell antenna has a horseshoe shape leading to an  $m = 0$  mode in the plasma [8], [15]. Rotational Type-III antenna was used by Okamura *et al.* [16] originally composed of four antenna elements placed around the plasma column. The relative phase of the RF current in each element is controlled, with one end of the antenna connected to the matching circuit, and the other end grounded. Shoji *et al.* [17] used an antenna with a helical form generating an  $m = \pm 1$  modes in the plasma. A first comparison of the electromagnetic properties among three different types of antennas was performed by Light and Chen [18] using both numerical simulations and experimentation. The three antennas were the Nagoya type-III antenna, with one having an  $m = \pm 1$  symmetry and plane polarization, while the other two, also type-III antennas have  $180^\circ$  helical twists instead of the straight horizontal legs [19]. It was found that the mode  $m = +1$  mode dominates for all excitation configurations. The flat spiral antenna with 3–4 turns was later used by different groups [20]–[23]. The power at 13.56 MHz is coupled *via* the flat spiral coil into an  $m = 0$  helicon mode. The novel feature of this source is an end-launch configuration without an externally defined parallel wavelength. In 1998, Miljak and Chen [24] conducted a study where the RF power was delivered by either one or two half-wavelength helical antennas, but no dramatic enhancement in the plasma density was detected. They also used a new design that is a phased bifilar antenna to excite helicon waves [25]. The plasma density and antenna loading measurements show that

Manuscript received 25 May 2022; revised 27 June 2022; accepted 4 July 2022. Date of publication 26 July 2022; date of current version 23 September 2022. This work was supported in part by the IAEA F1019 CRP on “Network of Small and Medium Size Magnetic Confinement Fusion Devices for Fusion Research” under Grant 22788 and in part by the AUB University Research Board Collaborative Research Stimulus under Grant 103782. The review of this article was arranged by Senior Editor J. G. Leopold. (*Corresponding author: Ghassan Antar.*)

Rayan AlSayed Ali and Joseph Costantine are with the Electrical Engineering Department, American University of Beirut, Beirut 1107-2020, Lebanon.

Ghassan Antar is with the Physics Department, American University of Beirut, Beirut 1107-2020, Lebanon (e-mail: ghassan.antar@aub.edu.lb).

Color versions of one or more figures in this article are available at <https://doi.org/10.1109/TPS.2022.3189579>.

Digital Object Identifier 10.1109/TPS.2022.3189579

0093-3813 © 2022 IEEE. Personal use is permitted, but republication/redistribution requires IEEE permission. See <https://www.ieee.org/publications/rights/index.html> for more information.

$m < 0$  waves are poorly coupled, and  $m = +1$  waves are necessary for good plasma production. Guittienne *et al.* [26] showed that a birdcage-type antenna is excellent for helicon  $m = 1$  mode excitation.

From the numerical simulations perspective, at first, antennas were modeled as thin wires [27]–[30]. Then, Melazzi and Lancelotti [31] introduced the ADAMANT code that solves the surface and volume integral equations for the analysis and design of helicon plasma sources. They conducted a comparative analysis of the single-loop, the Nagoya type-III, and the fractional helix (FH) antennas [32]. From the real and imaginary parts of the impedance, it was concluded that the single-loop out-performs the other two at low densities, and that the type-III Nagoya behaves better at higher magnetic fields. Stratakos *et al.* [33] used a commercially available full-wave 3-D electromagnetic analysis code (the CST microwave studio) to compare different antenna geometries. Four designs were discussed, that are, the two helical with  $N = 1$  and 4, the half, and the full Nagoya type-III antennas. Their findings indicate that the field increases and becomes more uniform when increasing the number of turns. In 2018, Fazelpour *et al.* [34] also used a commercially available, COMSOL Multiphysics 5.3 software, to investigate the wave pattern symmetry for a Nagoya type-III antenna. In contrast to the theoretical model prediction, the authors found that the electromagnetic wave presents an asymmetric pattern. They continued to propose a new configuration that increases the absorbed power and they predicted an increase of 40% of the plasma density. On the other hand, the ANSYS Electronics Desktop (AED) software, previously referred to as HFSS, was successfully used to simulate antennas for a variety of applications. We cite the CubeSat deployable antennas [35]–[37], the optically pumped reconfigurable antenna system [38], and the power transfer and wireless antenna system [39].

The main goal of this article is to show that there is a power-law relationship between the Gain of an antenna and the generated plasma density. This connection, obtained for the first time, should facilitate the future implementation of plasma RF sources. In Section III, we thus proceed by presenting the experimental results of the plasma properties for four different antennas using a Langmuir probe. This is followed by their electromagnetic properties obtained by numerical simulations. The main result of this article is discussed in Section V, which shows the power-law dependence of the plasma density on the Gain. To confirm this correlation, we design and build a new antenna, the modified quadrifilar helical (QH) antenna. We achieve not only a higher plasma density but also confirm the power-law dependence between the plasma density and the gain of an antenna.

## II. EXPERIMENTAL SETUP

### A. Polaris Device and the Four Antennas

Polaris is a linear plasma device that is operational at the American University of Beirut [40]. It consists of a stainless-steel chamber that is approximately 3 m long and 30 cm in diameter. The base pressure  $1.5 \times 10^{-7}$  bar is obtained by using a turbo and a backup scroll pump. The argon gas



Fig. 1. (a) Picture of the Polaris linear plasma device where one can see the 12 magnets with their power cables and the water cooling connections. (c) RF antenna with the matching network. (d) Pumping system. Also is visible, the window ports where the images in (c) and (d) are taken. (b) Fused silica window that acts as an end-plate where the Langmuir probe can be seen.

pressure inside the vacuum vessel is set and controlled by a mass-flow controller. The magnetic field is generated by a set of 12 water-cooled coils. The fact that the magnets as well as the RF power delivery (composed of the RF power supply, matching network, and antenna) are all water-cooled, allows us to operate continuously.

### B. RF Plasma Source

The RF source is set on the right-hand side of Polaris while on the left-hand side, we have a fused silica window that acts as an insulating end-plate [see Fig. 1(a)].

The helicon plasma source is composed of an RF power supply feeding an antenna through an impedance matching network. The RF power supply from Advanced Energy (AE), model RF-20S, is characterized by a 2000-W maximum output power and a fixed frequency of 13.56 MHz. The matching network, series AM-20, is used to transform a wide range of resistance and reactive impedance encountered during plasma generation, into the source impedance of  $50 \Omega$ . The matching network “L” configuration is composed of a variable shunt capacitor, with a maximum capacitance of 1000 pF, that handles the loading. In series, we have a fixed five-turn coil and a variable capacitor, with a maximum capacitance of 500 pF, that handles the tuning. The matching network has an “Auto-Manual-Remote” control switch that selects the mode of operation. However, the “manual mode” was adopted and the two variable capacitors are tuned using switches allowing us to achieve a maximum reflected power of 2% for any experiment.

The antenna is the component responsible for coupling the RF power into the plasma and driving the discharge by launching an RF wave. It is installed around a bell-shaped quartz tube, which has a diameter equal to 5 cm. It was shown



Fig. 2. (a)–(d) Pictures of the APS antenna, the PS antenna, the FH antenna, and the PFH antenna, respectively. The white arrows indicate the direction of the current at a given time. The two “horizontal” strips to the left of each antenna are dedicated to their connection to the matching network. One can see the copper tubes for water cooling soldered on the antennas.

that the magnetic field in the region where plasma is generated is rather uniform with values that can reach up to 750 G [40].

### C. Four Antennas

In this article, only the current paths of the antennas are different while the rest of the parameters are identical. The design of the four antennas is inspired by previous investigations. Their pictures are shown in Fig. 2 where the arrows indicate the directions of the current at a given instant. They share a common feature of having two loops connected by two strips, and the main difference is the current path in the loops or/and the geometry of the connecting arms. We use a 3-mm-thick copper sheet to perform a laser cut, which leads to strips with a width of 1.5 cm. Then, they are folded around an axis to have the same inner radius of  $a = 3.5$  cm and length  $L = 11$  cm. In terms of nomenclature, we call the antenna shown in Fig. 2(a) the “antiparallel straight” (APS) antenna because the current in the two loops flows in the opposite direction and the connection between the two loops is done with two parallel straight (PS) strips. The same type of connection is used in Fig. 2(b) but the current in the two loops is parallel, hence, it is called the “PS” antenna. The “FH” antenna, shown in Fig. 2(c), is similar to the Nagoya type-III antenna where the current in the loops is divided into two with opposite directions and they are connected by two helical strips. In Fig. 2(d), we have the “parallel FH” (PFH) antenna where the connecting strips have a helical form with the currents in the two loops parallel to each other.

For all the experiments presented in this article unless mentioned differently, we set the argon gas pressure to about

2 mtorr, the magnetic field at 600 G, and the RF power is 1000 W with a maximum reflected power of 20 W. The plasma is visually verified to be in the argon-blue mode reflecting good coupling of the helicon wave to the plasma and thus producing higher densities [9], [41]. Pictures of the plasma are shown in Fig. 1(b)–(d) taken, respectively, from the end-plate window, the side window, and through the bell-shaped quartz tube in the source region.

### D. Langmuir Probe

The plasma properties are deduced from the reciprocating Langmuir probe, also called an electric probe [40], [42], [43]. It is a tungsten rod with 1-mm diameter inserted into a boron-nitride ceramic tube leaving only a length of 1 mm exposed to the plasma. The wire is connected to a 50- $\Omega$  resistance and biased by a Kepco power supply with a voltage that is swept between  $-100$  and  $+5$  V in 1/2 ms. The measured potential drop around the resistance is proportional to the plasma current by Ohm’s law and as the latter is plotted as a function of the applied potential, we obtain the so-called IV trace. The floating potential of the different plasmas is about  $-5$  V, thus the bias range avoids the electron side of the IV trace, which would lead to overheating of the probe caused by high currents. The plasma electron temperature is deduced from the exponential increase around the floating potential where the current is zero. The plasma density is deduced from the ion saturation current after inserting the value of the electron temperature.

The electric probe is installed at about 2-m downstream from the source. It is thus expected to measure a lower density than in the source region but, on the other hand, the effects of the electromagnetic field on the probe measurement may be neglected. The axial dependence of the plasma properties was investigated in [19] and [24] using a straight quartz tube around which the antenna was installed. Thus, the radial plasma-wall interaction takes place along the whole plasma column. Axial plasma density variations were reported with a maximum that was reached between the source and the end plate. The origin of this behavior is still under investigation, but assuming that in the  $z$ -direction the electron pressure must be nearly constant, hence, the density rises in the downstream region simply because the temperature falls. Shinohara *et al.* [21] and Lee *et al.* [44] use a vacuum chamber similar to ours where the downstream region has radii greater than the plasma radius, hence, a strongly reduced radial contact between the plasma column and the walls. They reported a monotonous decrease of the density downstream from the source. In this article, we do not present the  $z$ -dependence of the plasma properties. However, since our setup is similar to the one in [14] and [44] and since all the geometric parameters are unchanged during the experiments, we shall assume that changing the antenna does not alter the gradient in the  $z$ -direction 2 m away from the source.

## III. EXPERIMENTAL RESULTS: THE PLASMA PROPERTIES USING THE FOUR ANTENNAS

### A. Plasma Properties for the Four Antennas

Fig. 3 shows the electron density in (a), and temperature in (b), as a function of the radial distance  $r$  to the plasma

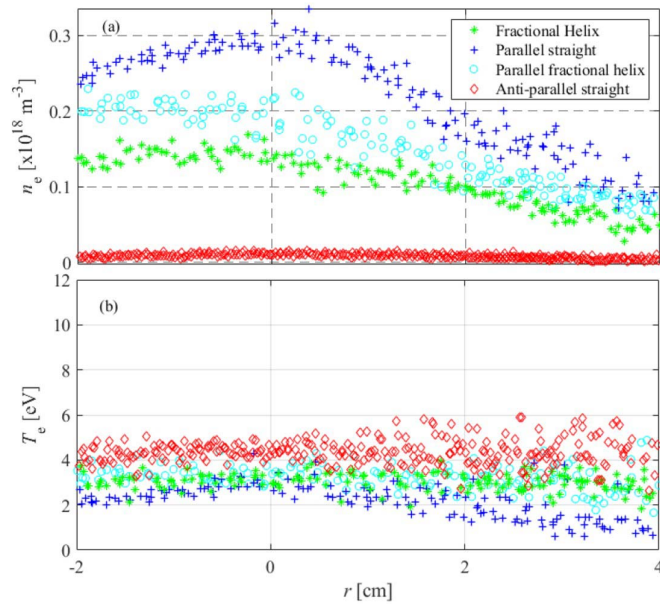


Fig. 3. (a) Electron density profile for the four different antennas obtained at the same input power of 1 kW and a reflection power that is less than 20 W. The highest plasma generation efficiency is reached when using the PS antenna. (b) Electron temperature is plotted as a function of  $r$  for the four antennas.

center for the four antennas. The plasma temperature is rather flat and changes slightly from one antenna to another. For this reason, we focus on the density behavior, which changes drastically from  $0.08 \times 10^{18} \text{ m}^{-3}$ , for the PFH antenna to  $0.3 \times 10^{18} \text{ m}^{-3}$  for the PS antenna indicating the importance of the current path in plasma generation. These changes are well above the experimental error of the measurement.

We thus emphasize the strong dependence of the plasma generation on the current path in the antenna. The goal of this present work is to find the relationship between the efficiency of the plasma generation and the antenna properties, which are deduced using numerical simulations.

#### IV. ANTENNAS CHARACTERIZATION USING NUMERICAL SIMULATION

This section is dedicated to the numerical simulation results to characterize the antenna's shapes. The simulation is done assuming that antennas are in a vacuum. Hereafter, we discuss first their radiation patterns before justifying the usage of Gain as a measure of the antenna property.

##### A. Radiation Patterns of the Electromagnetic Field

We use a commercially available program to characterize the four antennas. The first step is to have their 3-D CAD drawings. They are modeled to be composed of 3-mm-thick copper conductors as it is in reality. The drawings of the four antennas are shown in Fig. 4(a1)–(d1), respectively, for the APS, PS, FH, and PFH antennas.

We simulate the electromagnetic radiation properties using AED [45] at a radial distance where the plasma is expected. The modeled antennas were verified to match well at

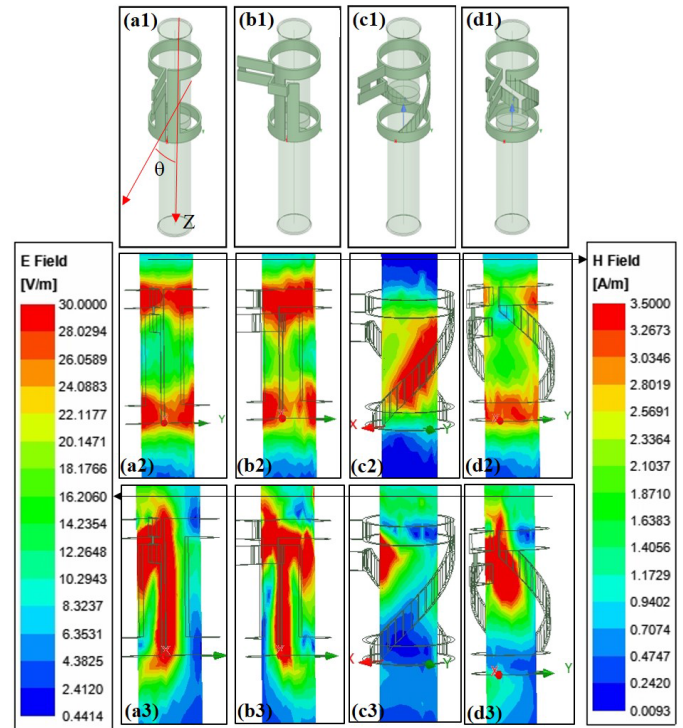


Fig. 4. (a1)–(d1) 3-D CAD drawings, respectively, for the four antennas the APS, PS, FH, and PFH. We denote by  $Z$  the direction of the antenna's axis and by  $\theta$  the angle with respect to this axis. (a2)–(d2) Magnetic field amplitude generated by the four antennas at the distance of the inner surface of the quartz tube. The color bar to the right-hand side indicates the color-to-amplitude conversion. (a3)–(d3) Similar but for the electric field, where the color bar to the left is dedicated to the color-to-amplitude conversion. We note that the strips that connect the antennas to the matching network enhance the electric field.

13.56 MHz with a bandwidth of 1.85 MHz. The magnetic field radiation for the four antennas is shown in Fig. 4(a2)–(d2). The PS and APS antennas present similarities with the magnetic field amplitude reaching maxima at the axial locations of the two loops. For the helical antennas, the maximum appears to move toward the center in-between the two loops. The electric field radiation is shown in Fig. 4(a3)–(d3) for the four antennas. A high electric field is achieved in areas facing the connecting strips between the two loops when the “straight” configuration is used. For the helical strip antennas, the maximum electric field is reached in the region facing the location where the connection to the matching network takes place.

From the simulation of the radiated electric and magnetic fields, we determine their respective average energy by integrating over  $\theta$ . We plot the two quantities as a function of the axial direction  $Z$  in Fig. 5(a) and (b), respectively. The four antennas present similar electrical energy dependence on  $Z$ . The peak at positive  $Z$ 's is caused by the strips dedicated to the connection to the matching network. The maxima of the energy per unit volume are attained at the same axial distance from the center and are between 2 and 4 nJ/m<sup>3</sup> depending on the type of antenna used.

The average magnetic field energy density is plotted in Fig. 5(b). It appears not to be sensitive to the asymmetry of

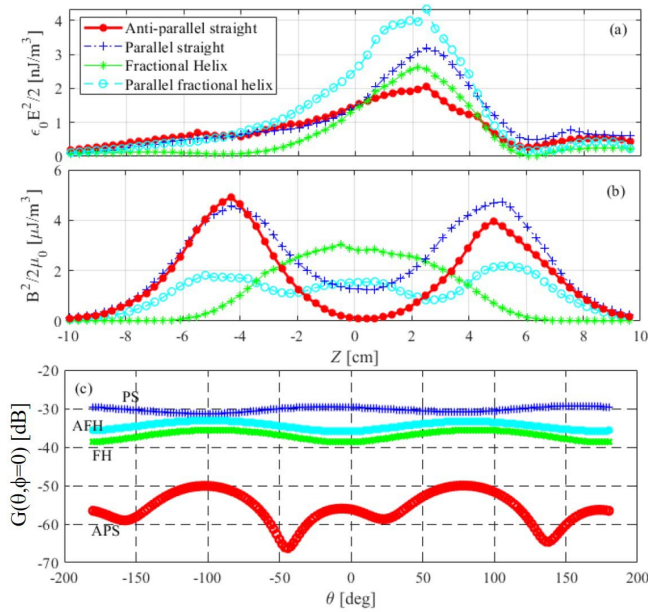


Fig. 5. (a) Electric energy density averaged over the azimuthal angle as a function of the axial position, for  $\phi = 0$ , with maxima reached where the connection to the matching network takes place. (b) Same color and markers to show the magnetic energy density as a function of  $Z$ . (c) Gain in dB as a function of the azimuthal angle  $\theta$  for the four antennas.

the design due to the matching network connection. The axial dependence of the magnetic energy is symmetric with respect to  $Z = 0$  and yields a clearer representation than the 3-D plots in Fig. 4(a2)–(d2). The maximum of the magnetic energy, which is about  $3 \mu\text{J/m}^3$ , occurs on the  $z$ -axis where the two loops are located ( $Z = \pm 5$  cm) for the straight parallel and antiparallel antennas. It is more uniform for the PFH antenna and peaks in-between the two loops, at  $Z = 0$ , for the FH. The magnetic energy being about 1000 times greater than the electric energy supports the assumption that inductive coupling of the electromagnetic waves dominates the plasma generation.

### B. Quantifying the Antennas Performance by Its Gain

When installed on the Polaris linear plasma device, the antennas engulf the cylindrical vacuum tube at a distance of about 1 cm from every side. They inductively couple the electromagnetic energy into this tube, which results in plasma generation. One of the main and common properties of an antenna is its Gain,  $G(\theta, \phi)$ , defined in spherical coordinates, where  $\theta$  is the angle between the  $z$ -axis and the vector from the origin to the point in space, and  $\phi$  is the angle between the  $x$ -axis and the projection of the point onto the  $(xy)$  plane [see Fig. 4(a)]. It is the ratio of the peak power radiated at a given angle  $P_r(\theta, \phi)$  normalized by the total injected power  $P_{\text{in}}$  [46]. Consequently, we have

$$G = 4\pi \frac{P_r(\theta, \phi)}{P_{\text{in}}}, \quad \text{where } P_r = \frac{c}{2} \left( \epsilon_0 E^2 + \frac{1}{\mu_0} B^2 \right). \quad (1)$$

The Gain of an antenna is a key characteristic that defines its radiative performance in the far-field. The dependence of  $G$  on  $\theta$  for the four different antennas is plotted in Fig. 5(c)

TABLE I

GAIN AND THE MAXIMUM PLASMA DENSITIES FOR THE FOUR ANTENNAS

	APS	PS	FH	PFH
$G_M$ [dB]	-50	-29	-37	-33
$n_e(r=0)$ [ $10^{18} \text{ m}^{-3}$ ]	0.03	0.28	0.13	0.24

assuming that they are radiating in a vacuum. They show different levels as well as different dependencies on  $\theta$ . The values obtained are far from unity reflecting strong anisotropy in the radiated far-field. Their sizes being about 1/200 the RF wave wavelength (22.12 m) allows us to consider them as infinitesimal antennas, consequently, from the simulation standpoint,  $G$  is well defined. Hereafter, we refer to the Gain of an antenna as being the maximum achieved for all values of  $\theta$  and  $\phi$ ,  $G_M = \max(G)$ . The values of  $G_M$  are inserted in Table I for the four antennas as obtained from the numerical simulation.

The four antennas have different Gain values varying from  $-50$  dB for APS to  $-30$  dB for the PS depending on the choice of the current path. The negative Gain obtained from the simulations is expected since the goal is not to radiate electromagnetic fields to the far-field, but rather to couple these fields inductively into the plasma that is about 1 cm away from the antenna.

### V. PLASMA DENSITY DEPENDENCE ON THE GAIN OF THE ANTENNA

On one hand, we use the Langmuir probe to measure the plasma properties for the four antennas, and on the other, a commercially available numerical simulation code to characterize their Gain. In this section, we aim at finding the relationship between these two quantities. We select the maximum of the plasma density reached at  $r = 0$  from the experiment. From the simulation, we select  $G_M$ , which is the maximum Gain as a function of  $\theta$  and  $\phi$ .

In Fig. 6(a), we plot  $n_e(r = 0)$  at  $B = 600$  G as a function of the  $G_M$  obtained from the numerical simulation in a log-log plot.

We note the linear increase of the plasma density with the Gain in this log-log plot, yielding the power law

$$n_e \sim G_M^{\zeta=0.5}. \quad (2)$$

This indicates that higher directionality leads to higher plasma density. This law allows us, and for the first time, to predict the plasma density once the Gain of an antenna is calculated using numerical simulation.

The above power law is obtained with all the plasma parameters set to constant and only the current paths in the antennas are different. To emphasize the universality of the above result, we change the magnetic field strengths, which modifies the plasma properties over relatively a wide range. We stress that in all of these experiments, the plasma remains in the ‘‘argon blue’’ mode. The plasma density is plotted as a function of the Gain for the four antennas and the different magnetic fields in Fig. 6(b). The scaling exponent  $\zeta$  is calculated and plotted in Fig. 6(c) against  $B$ , where we can

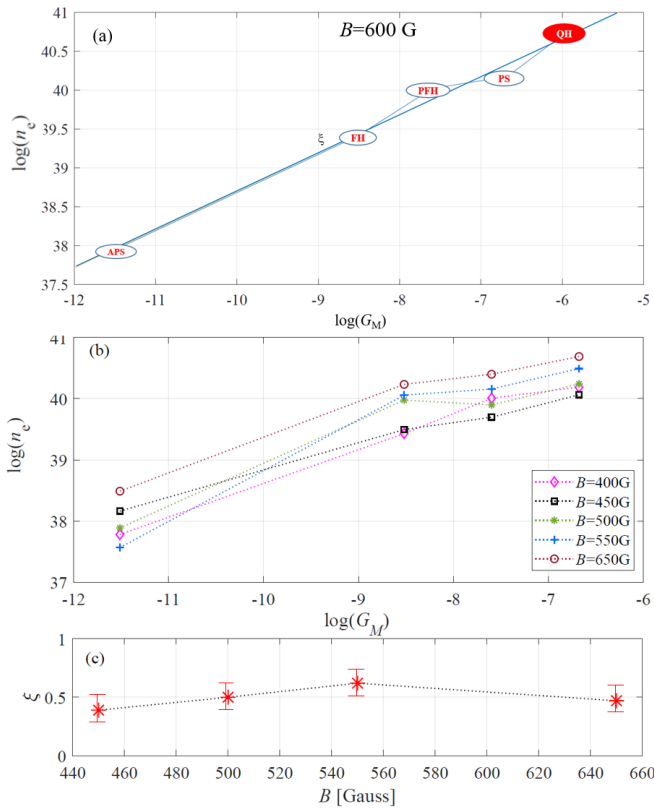


Fig. 6. (a) Density at  $r = 0$  as a function of the Gain for the four antennas with values inserted in white ellipses. The value for the modified quadrifilar antenna is shown by the red ellipse for the magnetic field equals to 600 G. (b) Plasma density as a function of the Gain of the four antennas in a log-log plot for magnetic fields ranging from 400 up to 650 G. For each dependence, we determine the scaling exponent  $\zeta$ , which is plotted in (c) where we show that it does not depend on  $B$  and thus on the plasma properties.

safely deduce that  $\zeta$  maintains a value of about 0.5. This result indicates that the power-law holds for at least the range of the plasma parameters, modified by changing  $B$ , investigated here.

In this section, we show that the plasma density dependence on the Gain of the antennas takes a form of a power law with a scaling exponent of about 1/2. We also succeeded to show that this scaling exponent does not depend on the plasma properties, which are modified by altering the magnetic field strength.

## VI. TESTING THE POWER-LAW WITH A NEW MODIFIED QUADRIFILAR HELIX SHAPE ANTENNA

The goal of this section is relatively straightforward as we aim at designing a new antenna that has a higher Gain and to verify that it produces a higher plasma density following the above power law. We thus emphasize that the design, fabrication, and testing of this new antenna is done after the results with the four more conventional antenna geometries.

A higher Gain is achieved by a novel design using a modified QH topology shown in Fig. 7. It has the same dimensions as the four double loop ones, which are a radius of 3.5 cm and a length of 11 cm. We use the same type of copper sheet and the same construction procedure. As shown

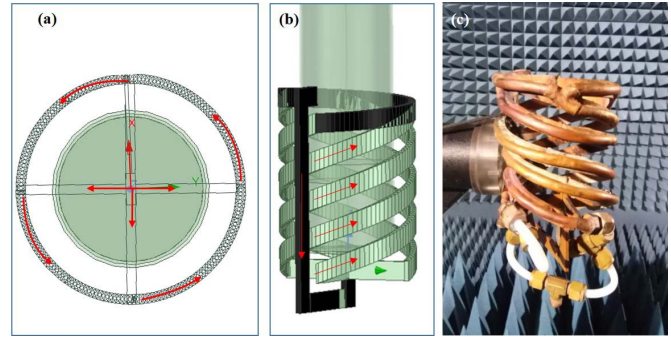


Fig. 7. Design of the modified quadrifilar antenna, which is composed of four helical arms that connect to a single helix. (a) View from the back of the antenna where the current is divided into equal four equal parts. (b) Side view shows the four helical almost full-wavelength turns. (c) Picture of the antenna where the water cooling copper pipes are visible.

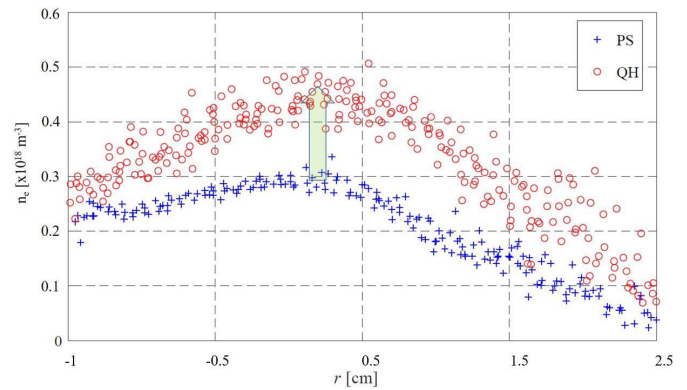


Fig. 8. Plasma density as a function of radius for the new modified QH antenna in “circ.” For comparison, we plot in “+” the density for the PS antenna with the best performance among the four antennas studied above.

in Fig. 7(a), the current in the antenna is divided into four equal parts by a junction that is linked to four arms. Each arm makes approximately a full turn in a helical form as can be seen in Fig. 7(b). The four helices join to another helix, which is grounded by a straight strip. As in the four antennas described previously, the water cooling tube is welded on the side of the copper sheet that is not facing the plasma.

This modified QH antenna is modeled and simulated. At the resonant frequency of 13.56 MHz, the input impedance of the antenna is equal to  $Z_i = 14.08j \Omega$ . The matching network placed in series between the antenna and the power supply ensures excellent matching with a total reflected power of about 20 W for 1000 W of injected power.

The Gain of the modified QH antenna exhibits a maximum  $G_M = -26$  dB, which is greater than the other four configurations. According to the scaling law obtained in 2, it is expected that it should lead to even higher plasma densities. To test its performance in plasma generation, we use the same Langmuir probe and the same experimental conditions on the Polaris linear plasma device. In Fig. 8, we plot the plasma density as a function of the radius  $r$  for the PS, which has shown the best performance, and the modified QH antenna. The quadrifilar helix antenna yields a plasma density of  $0.45 \times 10^{18} \text{ m}^{-3}$  that is 50% greater than PS antenna with  $0.3 \times 10^{18} \text{ m}^{-3}$ . This

proves that higher Gain in the numerical simulator leads to higher plasma density experimentally. Moreover, as we insert the plasma density obtained versus the Gain in Fig. 6(a), it becomes clear that it confirms the power-law dependence obtained using the four double-loop antennas.

## VII. CONCLUSION

Electromagnetic waves are launched to generate plasmas for a variety of applications. Important advances were reported showing an increase in the ionization process. Antennas are used to inductively couple the waves to the plasma with an efficiency that is relatively high when compared with other methods. It is known that the design of the antenna, namely the current path, plays an important role in enhancing the coupling efficiency. To address this issue in a rather systematic fashion, we designed four different antennas with the same dimensions but different current paths. The plasma density is measured on the Polaris linear plasma device using a Langmuir probe under the same experimental conditions, and we find that it strongly depends on the antenna type.

Advances in numerical simulations of the antenna electromagnetic field serve to evaluate the performance of any antenna design with accuracy. In this article, we take advantage of these advances to characterize the proposed antennas by their respective Gain even though they are used for inductive coupling rather than for radiation. Between the plasma density, obtained experimentally, and the Gain from the numerical simulation, the following law is obtained:

$$n_e \sim G_M^{0.5}$$

Moreover, we show that this law does not depend on the plasma properties, which are modified by changing the magnetic field.

To validate *a posteriori* this relationship, and thus to demonstrate its predictive capability, a new modified quadrifilar helix antenna is designed to have a Gain that is higher than the other four elements. This new current path leads to: (1) denser plasmas and (2) confirms the power law that links the gain to the plasma density.

The results of this article promise to transform the issue of plasma generation by RF waves into an antenna design problem that can be relatively easily modeled, optimized, and tested under vacuum conditions. It is the first time that such a relationship has been proven and tested experimentally. An advancement that is to our knowledge first of its kind.

Future work should be dedicated to understanding the origin of this relation between a far-field quantity, the Gain, and the plasma generation that occurs by the near-field coupling. We also need to investigate whether other antenna parameters could play a role in the increase of the plasma density for a given input RF power.

## ACKNOWLEDGMENT

The authors would like to thank A. Lalti and M. O. Ishtiak for their help and fruitful discussions.

## REFERENCES

- [1] G. Y. Antar, J. H. Yu, and G. Tynan, "The origin of convective structures in the scrape-off layer of linear magnetic fusion devices investigated by fast imaging," *Phys. Plasmas*, vol. 14, no. 2, Feb. 2007, Art. no. 022301.
- [2] S. N. Bathgate, M. M. M. Bilek, and D. R. McKenzie, "Electrodeless plasma thrusters for spacecraft: A review," *Plasma Sci. Technol.*, vol. 19, no. 8, 2017, Art. no. 083001.
- [3] J. Hopwood, "Review of inductively coupled plasmas for plasma processing," *Plasma Sources Sci. Technol.*, vol. 1, no. 2, p. 109, 1992.
- [4] F. F. Chen and R. W. Boswell, "Helicons—the past decade," *IEEE Trans. Plasma Sci.*, vol. 25, no. 6, pp. 1245–1257, Dec. 1997.
- [5] F. F. Chen, "Helicon discharges and sources: A review," *Plasma Sources Sci. Technol.*, vol. 24, no. 1, 2015, Art. no. 014001.
- [6] S. Shinohara, "Helicon high-density plasma sources: Physics and applications," *Adv. Phys. X*, vol. 3, no. 1, pp. 186–221, 2018.
- [7] J. Lehane and P. Thonemann, "An experimental study of helicon wave propagation in a gaseous plasma," *Proc. Phys. Soc.*, vol. 85, no. 2, p. 301, 1965.
- [8] R. W. Boswell, "Plasma production using a standing helicon wave," *Phys. Lett. A*, vol. 33, no. 7, pp. 457–458, Dec. 1970.
- [9] E. E. Scime, A. M. Keesee, and R. W. Boswell, "Mini-conference on helicon plasma sources," *Phys. Plasmas*, vol. 15, no. 5, May 2008, Art. no. 058301.
- [10] F. F. Chen, "Plasma ionization by helicon waves," *Plasma Phys. Control. Fusion*, vol. 33, no. 4, p. 339, Apr. 1991.
- [11] A. Molvik, A. Ellingboe, and T. Rognlien, "Hot-electron production and wave structure in a helicon plasma source," *Phys. Rev. Lett.*, vol. 79, no. 2, p. 233, 1997.
- [12] F. F. Chen and D. D. Blackwell, "Upper limit to Landau damping in helicon discharges," *Phys. Rev. Lett.*, vol. 82, no. 13, p. 2677, 1999.
- [13] A. W. Trivelpiece and R. W. Gould, "Space charge waves in cylindrical plasma columns," *J. Appl. Phys.*, vol. 30, no. 11, pp. 1784–1793, 1959.
- [14] G. Chen, A. V. Arefiev, R. D. Bengtson, B. N. Breizman, C. A. Lee, and L. L. Raja, "Resonant power absorption in helicon plasma sources," *Phys. Plasmas*, vol. 13, no. 12, Dec. 2006, Art. no. 123507.
- [15] R. W. Boswell, "Very efficient plasma generation by whistler waves near the lower hybrid frequency," *Plasma Phys. Controlled Fusion*, vol. 26, no. 10, p. 1147, 1984.
- [16] S. Okamura *et al.*, "Plasma production with rotating ion cyclotron waves excited by Nagoya type-III antennas in RFC-XX," *Nucl. Fusion*, vol. 26, no. 11, p. 1491, 1986.
- [17] T. Shoji, Y. Sakawa, S. Nakazawa, K. Kadota, and T. Sato, "Plasma production by helicon waves," *Plasma Sources Sci. Technol.*, vol. 2, no. 1, pp. 5–10, Feb. 1993.
- [18] M. Light and F. F. Chen, "Helicon wave excitation with helical antennas," *Phys. Plasmas*, vol. 2, no. 4, pp. 1084–1093, Apr. 1995.
- [19] F. F. Chen, "Physics of helicon discharges," *Phys. Plasmas*, vol. 3, no. 5, pp. 1783–1793, May 1996.
- [20] J. E. Stevens, M. J. Sowa, and J. L. Cecchi, "Helicon plasma source excited by a flat spiral coil," *J. Vac. Sci. Technol. A, Vac., Surf., Films*, vol. 13, no. 5, pp. 2476–2482, Sep. 1995.
- [21] S. Shinohara, S. Takechi, and Y. Kawai, "Effects of axial magnetic field and Faraday shield on characteristics of RF produced plasma using spiral antenna," *Jpn. J. Appl. Phys.*, vol. 35, no. 8R, p. 4503, 1996.
- [22] S. Shinohara and T. Tanikawa, "Development of very large helicon plasma source," *Rev. Sci. Instrum.*, vol. 75, no. 6, pp. 1941–1946, Jun. 2004.
- [23] S. Shinohara *et al.*, "Development of high-density helicon plasma sources and their applications," *Phys. Plasmas*, vol. 16, no. 5, pp. 057104-1–057104-10, May 2009.
- [24] D. G. Miljak and F. F. Chen, "Density limit in helicon discharges," *Plasma Sources Sci. Technol.*, vol. 7, no. 4, p. 537, 1998.
- [25] D. G. Miljak and F. F. Chen, "Helicon wave excitation with rotating antenna fields," *Plasma Sources Sci. Technol.*, vol. 7, no. 1, p. 61, 1998.
- [26] P. Guittienne, E. Chevalier, and C. Hollenstein, "Towards an optimal antenna for helicon waves excitation," *J. Appl. Phys.*, vol. 98, no. 8, Oct. 2005, Art. no. 083304.
- [27] Y. Mouzouris and J. E. Scharer, "Modeling of profile effects for inductive helicon plasma sources," *IEEE Trans. Plasma Sci.*, vol. 24, no. 1, pp. 152–160, Feb. 1996.
- [28] F. F. Chen and D. Arnush, "Generalized theory of helicon waves. I. Normal modes," *Phys. Plasmas*, vol. 4, no. 9, pp. 3411–3421, 1997.
- [29] D. Arnush and F. F. Chen, "Generalized theory of helicon waves. II. Excitation and absorption," *Phys. Plasmas*, vol. 5, no. 5, pp. 1239–1254, 1998.

- [30] I. V. Kamenski and G. G. Borg, "A 1D cylindrical kinetic wave code for helicon plasma sources," *Comput. Phys. Commun.*, vol. 113, no. 1, pp. 10–32, Sep. 1998.
- [31] D. Melazzi and V. Lancellotti, "ADAMANT: A surface and volume integral-equation solver for the analysis and design of helicon plasma sources," *Comput. Phys. Commun.*, vol. 185, no. 7, pp. 1914–1925, Jul. 2014.
- [32] D. Melazzi and V. Lancellotti, "A comparative study of radiofrequency antennas for helicon plasma sources," *Plasma Sources Sci. Technol.*, vol. 24, no. 2, 2015, Art. no. 025024.
- [33] Y. Stratakos, A. Zeniou, and E. Gogolides, "Comparison of helical and helicon antennas as sources of plasma excitation using a full wave 3D electromagnetic analysis in vacuum," *Plasma Processes Polym.*, vol. 14, nos. 4–5, 2017, Art. no. 1600107.
- [34] S. Fazelpour, A. Chakhmachi, D. Iraj, and H. Sadeghi, "Design and simulation of NBI heating system using high dense helicon plasma source for Damavand tokamak," *Fusion Eng. Des.*, vol. 137, pp. 152–164, Dec. 2018.
- [35] J. Costantine, Y. Tawk, C. Christodoulou, S. Barbin, J. Banik, and S. Lane, "Merging reconfigurable and deployable antennas for space applications," in *IEEE MTT-S Int. Microw. Symp. Dig.*, Oct. 2011, pp. 905–909.
- [36] J. Costantine, Y. Tawk, C. G. Christodoulou, J. Banik, and S. Lane, "CubeSat deployable antenna using bistable composite tape-springs," *IEEE Antennas Wireless Propag. Lett.*, vol. 11, pp. 285–288, 2012.
- [37] J. Costantine *et al.*, "UHF deployable helical antennas for CubeSats," *IEEE Trans. Antennas Propag.*, vol. 64, no. 9, pp. 3752–3759, Sep. 2016.
- [38] Y. Tawk, J. Costantine, S. Hemmady, G. Balakrishnan, K. Avery, and C. G. Christodoulou, "Demonstration of a cognitive radio front end using an optically pumped reconfigurable antenna system (OPRAS)," *IEEE Trans. Antennas Propag.*, vol. 60, no. 2, pp. 1075–1083, Feb. 2012.
- [39] R. Shadid, M. Haerinia, and S. Noghianian, "Study of rotation and bending effects on a flexible hybrid implanted power transfer and wireless antenna system," *Sensors*, vol. 20, no. 5, p. 1368, Mar. 2020.
- [40] G. Antar, J. Younes, M. Darwish, J. Costantine, M. Roumieh, and C. Habchi, "The polaris linear plasma device," *IEEE Trans. Plasma Sci.*, vol. 49, no. 5, pp. 1706–1713, May 2021.
- [41] C. Wang, Y. Liu, M. Sun, T. Zhang, Q. Chen, and H. Zhang, "Effect of inhomogeneous magnetic field on blue core in AR helicon plasma," *Phys. Plasmas*, vol. 28, no. 12, Dec. 2021, Art. no. 123519.
- [42] I. H. Hutchinson, *Principles of Plasma Diagnostics*, 2nd ed. Cambridge, U.K.: Cambridge Univ. Press, 2002.
- [43] G. Antar, A. Bahja, N. Metni, and C. Habchi, "The effect of adding an axial magnetic field on the expansion of a laser-produced plasma," *Phys. Plasmas*, vol. 26, no. 4, Apr. 2019, Art. no. 043515.
- [44] C. A. Lee, G. Chen, A. V. Arefiev, R. D. Bengtson, and B. N. Breizman, "Measurements and modeling of radio frequency field structures in a helicon plasma," *Phys. Plasmas*, vol. 18, no. 1, Jan. 2011, Art. no. 013501.
- [45] ANSYS HFSS, Version 13, Ansoft Corp., Pittsburgh, PA, USA, 2011.
- [46] C. A. Balanis, *Antenna Theory: Analysis and Design*. Hoboken, NJ, USA: Wiley, 2005.



**Rayan AlSayed Ali** received the B.E. and M.E. degrees from the American University of Beirut, Beirut, Lebanon, in 2017 and 2020, respectively, where she is currently pursuing the Ph.D. degree with the Electrical and Computer Engineering Program.

Her main research interests include electromagnetics, antennas, design and fabrication of RF-based sensors for noninvasive, continuous monitoring of biomarkers, signal processing, and data analysis.



**Ghassan Antar** received the Ph.D. degree from the Ecole Polytechnique, Palaiseau, France, in 1997.

He is currently a Professor at the Physics Department, American University of Beirut (AUB), Beirut, Lebanon, where he is also the Principle Investigator of the Polaris linear plasma device in operation. He has published more than 70 articles in peer-reviewed journals and is a referee to many international journals. His research interests include fluid dynamics with a focus on two and quasi-2-D turbulent flows applied to atmospheric geophysics.

He worked extensively on plasma physics in thermonuclear fusion devices on topics related to confinement and turbulence, liquid metals interaction with plasmas, edge, and scrape-off layer physics.



**Joseph Costantine** (Senior Member, IEEE) received the Ph.D. degree from The University of New Mexico, Albuquerque, NM, USA, in 2009.

He is currently an Associate Professor at the Electrical and Computer Engineering Department, American University of Beirut, and a World Economic Forum Young Scientist. He has 11 provisional and full U.S. patents. He has published two books, one book chapter, and more than 160 journal articles and conference papers. His research interests include reconfigurable antennas, cognitive radio, RF energy harvesting systems, antennas and rectennas for the Internet of Things devices, RF systems for biomedical devices, wireless characterization of dielectric material, and deployable antennas for small satellites.

Dr. Costantine received many awards and honors, including the 2008 IEEE Albuquerque Chapter Outstanding Graduate Award, the 2017 First Prize at the Idea-thon of International Healthcare Industry Forum, the 2020 STC Science and Technology Innovation Awards, and the 2020 distinguished Young Alumni Award from The University of New Mexico. He has been an Associate Editor of the IEEE ANTENNAS AND WIRELESS PROPAGATION LETTERS since July 2018.